Volume 1 | Number 1 | Jan 2013 | Pages 1–100

CrystEngComm

www.rsc.org/crystengcomm

ROYAL SOCIETY OF CHEMISTRY

ROYAL SOCIETY OF CHEMISTRY

www.rsc.org/crystengcomm

Synthesis of Self-Ordered and Well-Aligned Nb$_2$O$_5$ Nanotubes

Vardan Galstyan,* Elisabetta Comini, Guido Faglia and Giorgio Sberveglieri

Sensor Lab, Department of Information Engineering, University of Brescia and CNR INO, Via Valotti 9, 25133 Brescia, Italy

*E-mail: vardan.galstyan@unibs.it

Abstract

In the present work we demonstrate fabrication of self-assembled and highly-aligned Nb$_2$O$_5$ nanotubes by means of electrochemical anodization of metallic Nb at room temperature. We have investigated the effect of anodization parameters (the type and the concentration of the electrolyte, the anodization voltage and the current) on the formation of Nb$_2$O$_5$ nanotube arrays. The structural properties of nanotubes as a function of annealing treatment (temperature and duration) have been studied. The current-voltage characterization of the samples in dark and under the UV light illumination has been carried out. Photocurrent of the Nb$_2$O$_5$ nanotubes have been improved by improving their crystalline performance.

1. Introduction

Metal oxide self-ordered and vertically-oriented nanotubular arrays have stimulated great interests due to their potential technological application. The tubular shape is especially attractive since it can provide access to four different contact regions: tubes' inner and outer surfaces, top-side as well as the bottom of tubes. The materials unique architecture and large surface area make them promising structures for application in solar cells, gas sensors, energy storages, photocatalysis and medical materials.[1-11] Metal oxide nanoporous and nanotubular arrays can be formed by electrochemical oxidation reaction of metallic films under a specific conditions.[1, 12-15] It is very important to find best parameters for anodic formation of tub-like structures of each metal oxide. The formation of the tub-like structures during anodization is the result of a competition between the oxidation of the metal at the oxide/metal interface and oxide dissolution at the electrolyte/oxide interface. The rates of the oxidation and the dissolution reactions are strongly affected by the type of the electrolyte, the applied voltage and the anodization temperature.[1, 12, 13, 16] Therefore the anodization current density and the composition of the electrolyte solution are the key parameters for the transition of the obtained structure from porous to tubular arrays. The parameters of tubes (pore diameter, interpore distance, wall thickness and length of the tubes) can be tailored during the fabrication process at room temperature. Vertically aligned nanotubes are directly grown on the

substrate starting from a metallic titanium film or foil, without other precursors or assisting layers.[1, 6, 13, 17]

Formation of TiO_2 nanotubes by means of electrochemical anodization method in fluorine containing electrolyte was performed for the first time by Zwilling *et al*.[12, 18] TiO_2 nanotubular structure has been recognized as the most promising materials for solar cells and the photocatalytic reactions owing to its suitable band-edge position, wide band-gap (3.2 eV for anatase and 3 eV for rutile) and structure geometry. [19-22] Nb_2O_5 is a transition metal oxide with the band-gap of about 3.4 eV similar to that of TiO_2.[23] It has higher conduction band-edge compared to TiO_2 and could become an alternative material for application in catalysis, solar cells, chemical sensors, energy storages and photodetectors. [19, 20, 24-28] Nb_2O_5 is a good candidate for UV detectors due to its excellent photocurrent stability, UV light sensitivity and the high external quantum-efficiency.[28] Properties of the Nb_2O_5 photodetectors can be further optimized by mixing it with the potassium chloride (KCl) and fluorine (F).[29, 30]

Growth of self-organized Nb_2O_5 nanostructures by means of the electrochemical anodization method was demonstrated for the first time by Schmuki *et al*.[31] The prepared structures were porous. Further they demonstrated anodic formation of Nb_2O_5 nanotube arrays at room temperature[32]: however the authors have mentioned that the thickness of the structures was limited to a few hundreds of nms and the morphology was irregular.[33] By carrying out the anodization process at higher temperature ranges (160-200°C) highly ordered Nb_2O_5 nanochannels were produced with a pore diameter ranging between 20 and 50 nm.[33] All the other results in literature report anodized Nb_2O_5 structures which are only porous and of a limited thickness (~500 nm).[19, 31, 33-36] Ou *et al*. increased the thickness of the anodic porous Nb_2O_5 layer to ~4 μm by anodization of Nb foil at elevated temperatures:[19] a dye-sensitized solar cell based on the 4 μm Nb_2O_5 layer showed significantly higher efficiency (~4.1%) compared to that which incorporates a titanium dioxide nanotubular layer (~2.7%).[19]

Yan and Xue demonstrated another strategy for the synthesis of Nb_2O_5 nanotubes. They prepared nanotube arrays trough the transformation of Nb_2O_5 nanorods to nanotubes in Teflon-lined stainless steel autoclave at 230°C for 48 h.[23]

The results reported in literature confirm that Nb_2O_5 nanotubes are emerging as important materials and electrochemical anodization is a promised method for growing Nb_2O_5 nanotubes. Due to this reason the synthesis of Nb_2O_5 nanotube arrays and optimization of their parameters is a great challenge. Herein, we demonstrate the growth of self-assembled Nb_2O_5 nanotube arrays at room temperature optimizing their geometrical parameters. Thermal treatment induced amorphous-to-

crystalline phase transition and the impact of the structure crystallinity on its electrical properties have been investigated.

2. Experimental

Nb discs (0.5 mm thick, 9 mm diameter, with the average surface roughness (Ra) of 0.1 μm, 99,99 % purity, Goodfelow, England) were cleaned ultrasonically with acetone, ethanol and distilled water. Anodization of the specimens was carried out at room temperature in two-electrode system with the Pt foil as a counter electrode. The electrolyte solutions were H_2O and NH_4F (or FNa) containing glycerol and ethylene glycol. The concentrations of H_2O and NH_4F (FNa) were changed in the range of 0.5-25 M and 0.4-1.2 wt%, respectively. Experiments were performed at the potentials between 10 and 90 V for 5-90 min. using a power supply (Delta Elektronika SM 300-5). As-prepared structures were crystallized by thermal annealing at 400-500 °C in air for 20 and 60 min.

The morphology of the obtained structures was observed using a LEO 1525 scanning electron microscope (SEM) equipped with field emission gun. X-ray diffraction spectroscopy (XRD) was performed using an Empyrean diffractometer (PANalytical, Almelo, The Netherlands) mounting a Cu-LFF ($λ = 1.5406$ Å) tube operated at 40 kV and 40 mA. XRD spectra were recorded by a PIXcel 1D detector with a nickel large-β filter in scanning line detection mode with a Bragg-Brentano configuration. The diffraction angle was scanned between 10° and 80°, and a divergence slit of 1/16° was used obtaining a strong signal for relatively short acquisition times (1 hour).

For the current-voltage (I-V) characterizations Pt square electrodes (1 μm thick) were deposited on the specimens by means of RF magnetron sputtering. The distance between the metal electrodes is about 3 mm. Ultraviolet (UV) illumination of the samples was performed by UV spot light source (Hamamatsu L712-02, Japan) coupled with the 350 nm (FWHM 11±2nm) UV filter. I-V characterization of the samples was carried out by means of Keithley 2410 SourceMeter.

3. Results and discussions

Initially we have investigated anodization process of metallic Nb in comparatively viscose electrolyte solutions based on glycerol ($η = 945$ cP at 20 °C) and ethylene glycol ($η = 13.5$ cP at 20 °C).[37] Experiments determined that NH_4F and H_2O containing glycerol is the most promising solution for fabrication of Nb oxide nanotube arrays. We have studied the morphologies of the obtained structures and found that the decrease of H_2O concentration and increase of NH_4F content in glycerol are the key factors for the formation nanotubes. Therefore we carried out next experiments increasing the concentration of NH_4F in the range 0.8-1.1 wt% and setting H_2O content in the electrolyte to a value such low as 0.5 M. Morphological observations showed that the prepared structures are porous layers when the concentration of NH_4F in the electrolyte is less than

1.2 wt%. Figure 1 (a-c) shows SEM micrographs of the structure anodized in 0.8 wt% NH$_4$F and 0.5 M H$_2$O contained solution at 90 V. As can be seen in the cross-sectional image (Figure 1 (a)) and in the top-view (Figure 1 (b)) the structure is vein-like nanostructured network with the porous surface morphology. Figure 1 (c) shows a SEM image of the bottom of the porous layer that has been detached from the Nb substrate. The layer consist of semi-spheres in some parts connected with each other. The morphologies of the samples prepared in the electrolyte solution containing less than 1.2 wt% NH$_4$F at the potentials from 50 to 90 V were similar to that shown in Figure 1 while the samples anodized at the potentials lower than 50 V were comparably more disordered porous structures.

Figure 1 (d) reports the anodization current density transient recorded during anodization of the sample at 90 V. It does not exhibit the current density transient profile characteristic that is typical for the anodic formation of self-organized metal oxide nanoporous and nanotube arrays.[1, 31] Initially the current increases and reaches steady state. Then suddenly drops and increases again. These oscillations in the current density during the anodization process are related with the chemical dissolution and the electrochemical oxidation of the structure. The oscillations indicate that the equilibrium between the anodic oxide growth and the local oxide dissolution of the structure was not achieved during the anodization process. The results -vein-like structure with no tubular features- confirm that the equilibrium between the oxide growth and the dissolution is an important issue for the preparation of self-organized metal oxide nanotubes. [1, 31]
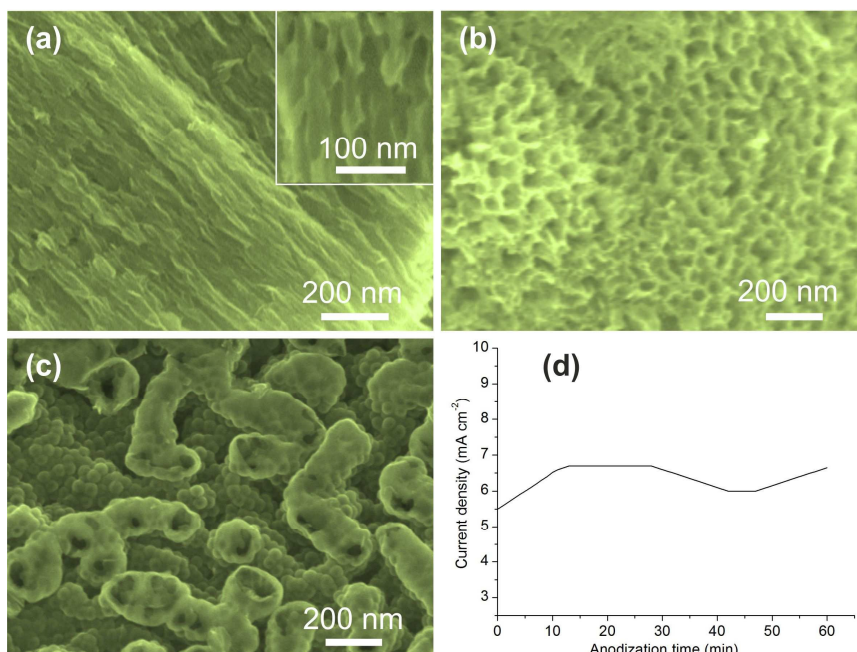

Figure 1. SEM images of the sample anodized in 0.8 wt% NH$_4$F and 0.5 M H$_2$O contained solution at 90 V. (a) The cross-sectional view of the anodized layer, (b) the surface morphology of the sample, (c) the bottom-view of the porous layer and (d) current density transients recorded during anodization.

We observed the transformation of the structures from porous to tubular arrays when H_2O concentration decreases to 0.5 M and the content of NH_4F increases to 1.2 wt%. Figure 2 (a-g) shows the SEM images of the structures anodized in 0.5 M H_2O and 1.2 wt% NH_4F containing solution at different potentials (30, 60, 80 and 90 V). The cross-sectional images show that the samples anodized at 30-60 V are not tubular, demonstrating that the applied potential is another key factor for the growth of Nb_2O_5 nanotube arrays. The tubes appeared when the anodization voltage was increased to 80 V and the best condition for the formation of self-organized and well-aligned nanotubes was found when the anodization potential was 90 V. As can be seen in the Figure 2 (d-g) well-aligned nanotubes with the length more than 5 μm are prepared. In the back-side and cross-sectional SEM images (Figure 2 (d) and (g)) is clearly seen that the anodized layer consists of well-separated individual nanotubes.

Figure 2 (h) reports the anodization current density transient recorded during the anodization of the samples at 30, 60, 80 and 90 V. The curves show the typical shape for self-organization processes. Initially the current decreases due to the formation of the compact oxide layer on the surface of Nb (eq. (1)).[38] Then current density increases due to the formation of pits in the oxide layer (eq. (2)) and in consequence of an equilibrium between the oxide growth and the chemical dissolution the current density reaches steady-stage.[1, 38] At this stage the pores grow into nanotubes as typical process for the anodic formation of self-organized metal oxide nanotubes.[1, 13]
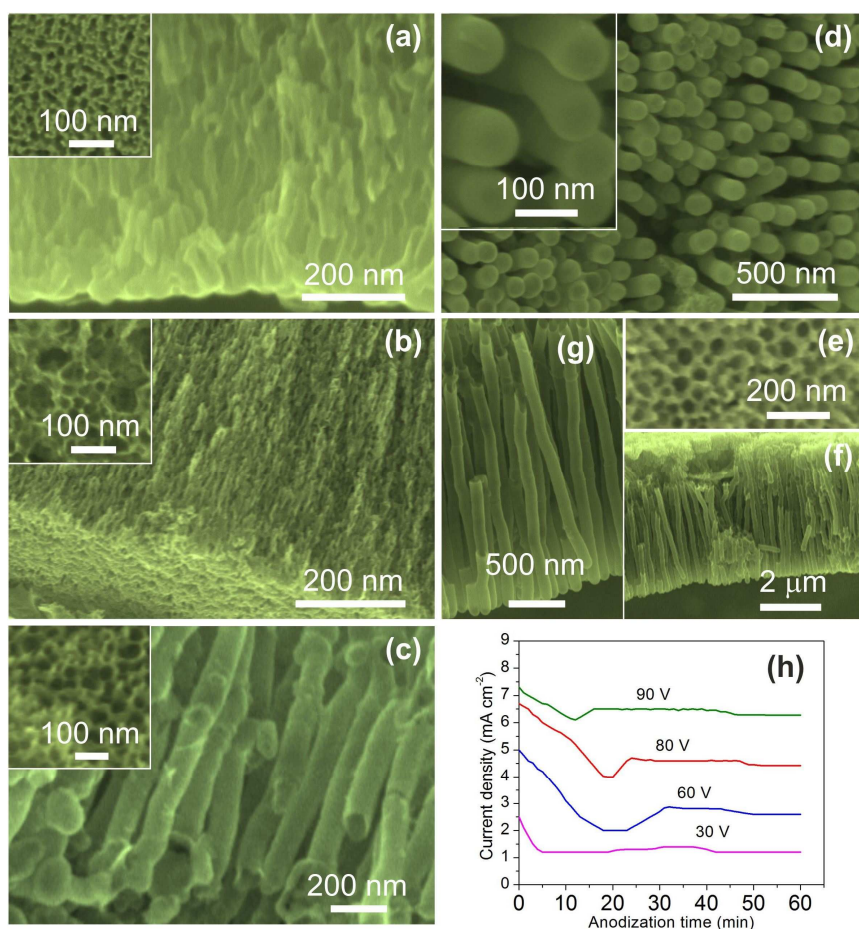
$$2Nb + 5H_2O \rightarrow Nb_2O_5 + 10H^+ + 10e^- \quad (1)$$

$$Nb_2O_5 + 10H^+ + 12F^- \rightarrow 2[NbF_6]^- + 5H_2O \quad (2)$$
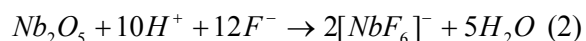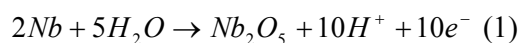
Figure 2. (a), (b) and (c) the cross-sectional views and the surface morphologies of the structures anodized in 0.5 M H_2O and 1.2 wt% NH_4F containing solution at the potentials of 30, 60 and 80 V, respectively. (d-g) SEM micrographs of the structure formed in 0.5 M H_2O and 1.2 wt% NH_4F containing solution at 90 V: (d) bottom-view (e) surface morphology, (f) and (g) cross-sectional view of nanotube arrays at low and high magnifications. (h) Current density transients recorded during the anodization at the potentials from 30 to 90 V.

Figure 3 shows the high resolution SEM images and the corresponding histograms of the internal and external tube diameter distribution for the as-prepared and annealed (at 450 °C for 60 min) Nb_2O_5 nanotubes. The average diameters were determined from the high resolution SEM images taken from different locations of the sample and by measuring 60 tubes. The average internal and external diameters of as-prepared nanotubes are 50 and 82 nm, respectively. The average internal and external diameters of nanotubes annealed at 450 °C for 60 min are 48 and 90 nm, respectively. The average internal and external diameter, and the relative standard deviation (RSD) of nanotubes annealed at different regimes are summarized in Table 1. The decrease of tube internal diameter and the increase of external diameter (resulting in a thicker tube-walls) of the annealed nanotubes is related with the increase of the crystals' size during the thermal treatment.[39] Similar morphology tuning after thermal annealing were also reported for TiO_2 nanotubes.[40]
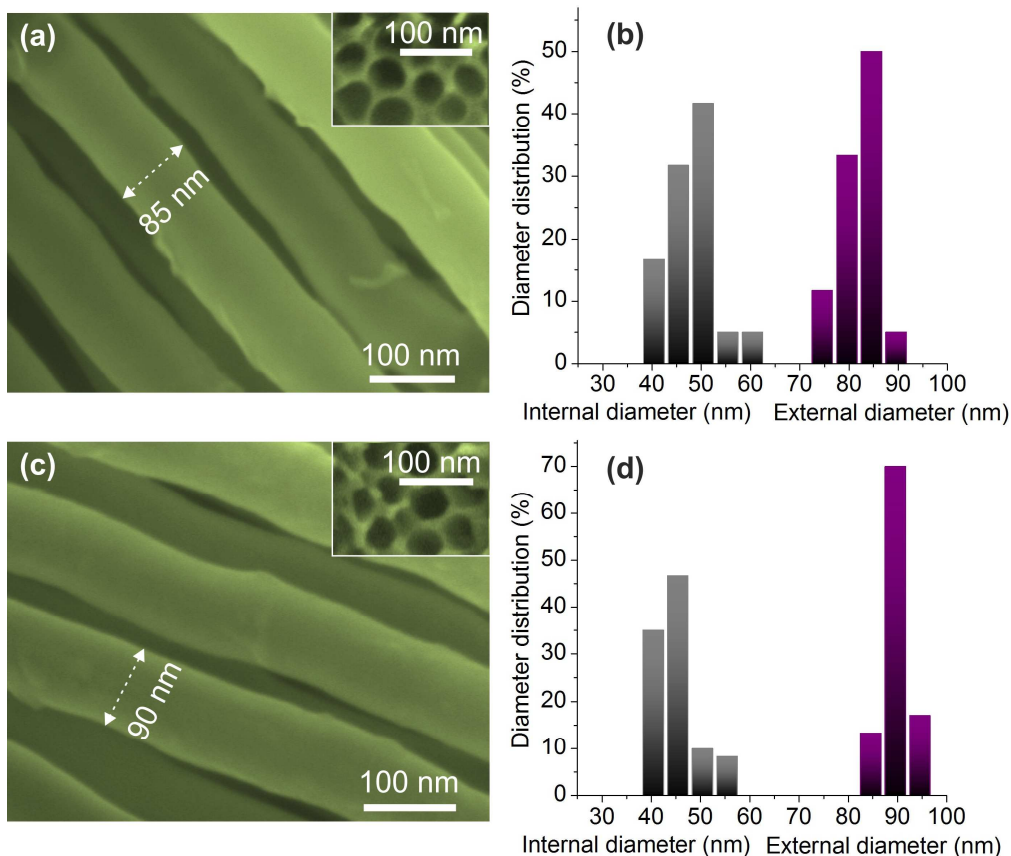
Figure 3. High resolution SEM images and the corresponding histograms of the internal and external tube diameter distribution of as-prepared and annealed nanotubes: (a) and (b) as prepared nanotubes, (c) and (d) nanotubes annealed at 450 °C for 60 min.

Table 1. Average internal and external diameters, and RSD of as-prepared and annealed (at 400, 450, 500 °C for 60 min) nanotubes.

Thermal treatment temperature	Average internal diameter (nm)	Average external diameter (nm)	RSD (%) for the internal diameter	RSD (%) for the external diameter
As-prepared	50	82	14	7
400 °C	48	87	12	2
450 °C	48	90	12	4
500 °C	42	90	13	3

Crystallographic information of niobium oxide nanostructures was analyzed with XRD. The as-prepared nanotubes are amorphous which is typical for Nb and other metal oxide nanostructures anodized at room temperature.[1, 4, 32, 41] The layers crystallize after heat treatments at or above 400°C. After the annealing treatments the layer is well crystallized and oxidized. Figure 4 (a) reports the XRD spectra for the samples annealed at different temperatures for 20 and 60 minutes.

Phases were identified according to ICDD- International Centre for Diffraction Data. The diffraction peaks were not changing at the different annealing temperature and times. The pattern was well fitted with JCPDS 27-1003 that corresponds to orthorhombic structure, however most of the main peaks of orthorhombic and hexagonal structure are so close that it's difficult to distinguish among these two phases precisely.
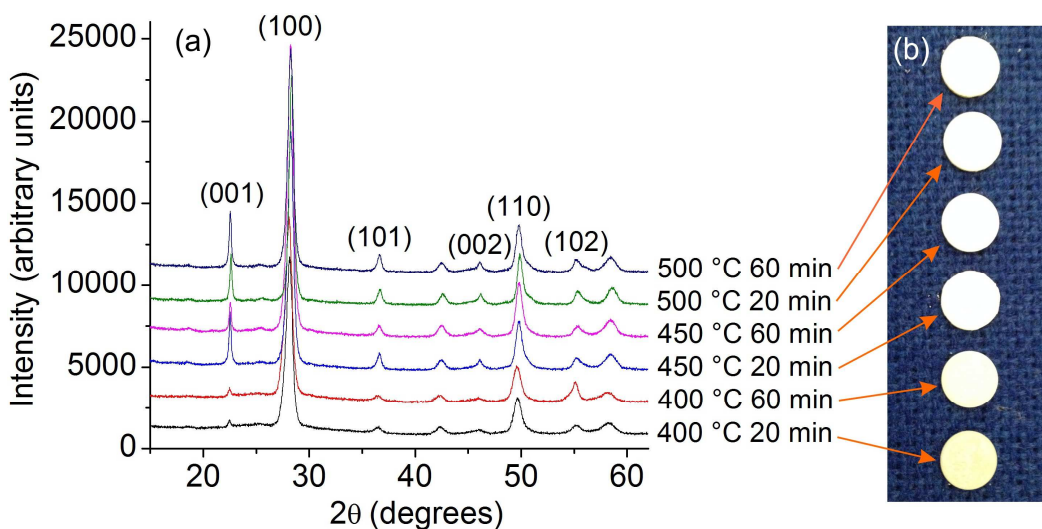

Figure 4. (a) XRD patterns of the samples annealed at 400-500 °C for 20 and 60 min. (b) Digital images of the samples crystallized at different annealing regimes.

In order to investigate the possible application of the structures for UV detection and photocatalysis we performed I-V characterizations in dark and under the UV illumination. Figure 5 (a) shows the I-V characterization of the Nb_2O_5 nanotube arrays annealed at 450 °C for 60 min. I-V plots were recorded in dark and under the UV illumination at the applied voltage of 1 V. The results of the measurements shows that the current value under the 350 nm UV illumination is more than two times higher compared to the current value in dark. The improvement of the current by the UV illumination is related with the desorption process of oxygen species on the surface of Nb_2O_5.[28, 42] When oxygen absorbs on the oxide surface, it captures the electrons form the conduction band and a negative space charge is created which results to the enhancement in the resistance ($O_2 + e^- \rightarrow O_2^-$).[42] When the structure was illuminated by the 350 nm (~3.54 eV) UV light, the photon energy was greater that band gap energy of Nb_2O_5 (3.4 eV) and electron-hole pairs were generated ($hv \rightarrow h^+ + e^-$). The created positively charged holes (h^+) neutralized the chemosorbed oxygen ($O_2^- + h^+ \rightarrow O_2$) and the structure conductance was increased. [28, 42]

I-V plots of the Nb_2O_5 nanotube arrays annealed at different regimes have shown similar characteristics to the plots reported in Figure 5 (a). The conductance of the samples annealed at different regimes and recorded in dark and under the UV illumination at the applied voltage of 1 V are reported in Figure 5 (b) and (c). Figure 5 ((b) and (c)) shows that the increase of conductance

due to the UV illumination for the samples annealed at 450 and 500 °C is much greater compared to the samples annealed at 400 °C. The crystallinity of the structures also improves with at higher annealing temperature (Figure 4). The results show that the photocurrent of the Nb_2O_5 nanotubular structure is improved by improving its crystallinity, in agreement with the results reported by Fang et al.[28] Meanwhile Nb_2O_5 based nanostructures demonstrate significant improvements in photodetectors performance compared to ZnO, ZnS and SnO_2.[27, 29, 43] Comparison of the current values of the obtained Nb_2O_5 nanotubes and the other semiconducting nanostructures recorded in dark and under the UV illumination is summarized in Table 2. [28, 43-46] Performance of the obtained Nb_2O_5 nanotubes makes them as good candidate as other oxides for developing UV photodetectors.
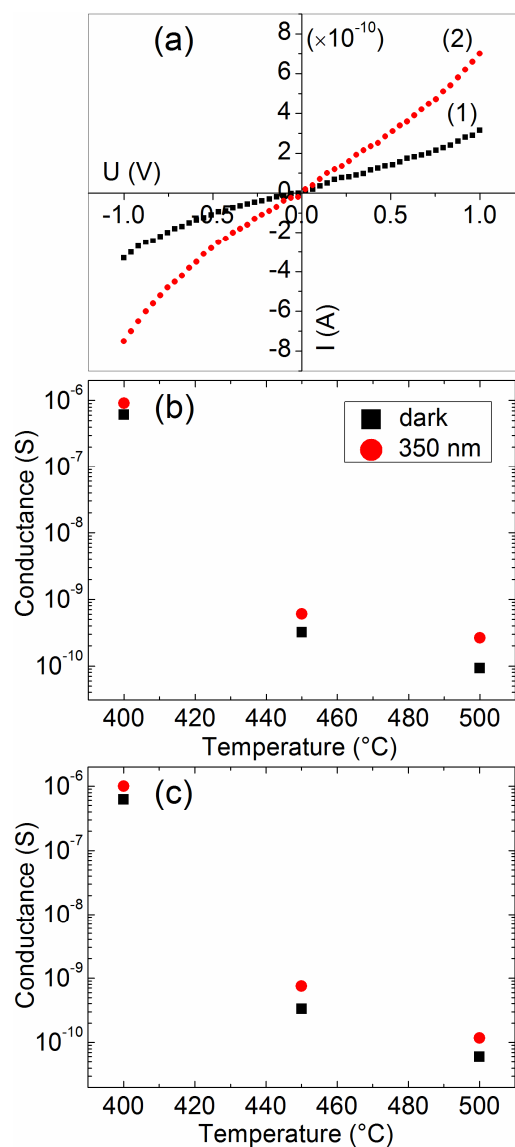

Figure 5. (a) I-V characterization of the Nb_2O_5 nanotube arrays annealed at 450 °C for 60 min: in dark plot (1) and with the 350 nm UV illumination plot (2). (b) and (c) the current values of the samples annealed at 400, 450 and 500 °C recorded in dark and under the UV illumination: (b) annealed for 20 min, (c) annealed for 60 min.

Table 2. Comparison of the key parameters of the obtained Nb_2O_5 nanotubes and the other semiconducting nanostructures recorded during the I-V characterization.

Structure	Applied voltage	UV light	Dark current	Photocurrent	Ref.
Nb_2O_5 nanobelt	1 V	320 nm	10.6 pA	100 pA	28
ZnS nanobelt	5 V	320 nm	<1 pA	1 pA	43
SnO_2 nanowires	1 V	350 nm	2.3 pA	0.5 nA	44
ZnO nanorods	2 V	325 nm	1 nA	22 nA	45
ZnO nanowires	1 V	365 nm	0.04 nA	60 nA	46
Nb_2O_5 nanotubes	1 V	350 nm	50 pA	100 pA	Present work

4. Conclusions

We have successfully fabricated self-ordered Nb_2O_5 nanotube arrays by means of electrochemical anodization method. Morphological analysis have shown that the increase of NH_4F concentration and the decrease of H_2O content in the electrolyte solution are crucial for the formation of highly-ordered porous structures and the applied voltage is a key factor for the growth of well-separated individual nanotubes. The XRD measurements indicated that amorphous-to-crystalline phase transformation of as-prepared nanotubes starts after the thermal treatment at 400 °C. The photocurrent of Nb_2O_5 nanotubes is enhanced by the improvement of the structure crystallinity. The obtained Nb_2O_5 tubular structure is good candidate for application in photocatalysis, photodetectors, solar cells, gas sensors and energy storages.

Acknowledgments

References

1. P. Roy, S. Berger and P. Schmuki, *Angewandte Chemie-International Edition*, 2011, **50**, 2904-2939.
2. O. K. Varghese, M. Paulose and C. A. Grimes, *Nature Nanotechnology*, 2009, **4**, 592-597.
3. V. Galstyan, A. Vomiero, I. Concina, A. Braga, M. Brisotto, E. Bontempi, G. Faglia and G. Sberveglieri, *Small*, 2011, **7**, 2437-2442.
4. V. Galstyan, E. Comini, G. Faglia, A. Vomiero, L. Borgese, E. Bontempi and G. Sberveglieri, *Nanotechnology*, 2012, **23**, 235706.
5. M. Paulose, O. K. Varghese, G. K. Mor, C. A. Grimes and K. G. Ong, *Nanotechnology*, 2006, **17**, 398-402.

6.   N. A. Kyeremateng, F. Vacandio, M. T. Sougrati, H. Martinez, J. C. Jumas, P. Knauth and T. Djenizian, *Journal of Power Sources*, 2013, **224**, 269-277.

7.   B. L. Ellis, P. Knauth and T. Djenizian, *Advanced Materials*, 2014, **26**, 3368-3397.

8.   A. Mazare, I. Paramasivam, K. Lee and P. Schmuki, *Electrochemistry Communications*, 2011, **13**, 1030-1034.

9.   S. Minagar, C. C. Berndt, J. Wang, E. Ivanova and C. Wen, *Acta Biomaterialia*, 2012, **8**, 2875-2888.

10.   P. Lv, W. Fu, H. Yang, H. Sun, Y. Chen, J. Ma, X. Zhou, L. Tian, W. Zhang, M. Li, H. Yao and D. Wu, *CrystEngComm*, 2013, **15**, 7548-7555.

11.   S. Grigorescu, V. Pruna, I. Titorencu, V. V. Jinga, A. Mazare, P. Schmuki and I. Demetrescu, *Bioelectrochemistry*, 2014, **98**, 39-45.

12.   V. Zwilling, M. Aucouturier and E. Darque-Ceretti, *Electrochimica Acta*, 1999, **45**, 921-929.

13.   V. Galstyan, A. Vomiero, E. Comini, G. Faglia and G. Sberveglieri, *RSC Advances*, 2011, **1**, 1038-1044.

14.   R. V. Goncalves, P. Migowski, H. Wender, A. F. Feil, M. J. M. Zapata, S. Khan, F. Bernardi, G. M. Azevedo and S. R. Teixeira, *CrystEngComm*, 2014, **16**, 797-804.

15.   A. M. M. Jani, D. Losic and N. H. Voelcker, *Progress in Materials Science*, 2013, **58**, 636-704.

16.   W. Lee, R. Scholz and U. Goesele, *Nano Letters*, 2008, **8**, 2155-2160.

17.   V. Galstyan, E. Comini, G. Faglia and G. Sberveglieri, *Sensors (Switzerland)*, 2013, **13**, 14813-14838.

18.   V. Zwilling and E. Darque-Ceretti, *Annales de Chimie*, 1997, **22**, 481-493.

19.   J. Z. Ou, R. A. Rani, M.-H. Ham, M. R. Field, Y. Zhang, H. Zheng, P. Reece, S. Zhuiykov, S. Sriram, M. Bhaskaran, R. B. Kanee and K. Kalantar-Zadeh, *ACS Nano*, 2012, **6**, 4045-4053.

20.   J. Z. Ou, R. A. Rani, M.-H. Ham, M. R. Field, Y. Zhang, H. Zheng, P. Reece, S. Zhuiykov, S. Sriram, M. Bhaskaran, R. B. Kaner and K. Kalantar-zadeh, *ACS Nano*, 2012, **6**, 5737-5737.

21.   D. O. Scanlon, C. W. Dunnill, J. Buckeridge, S. A. Shevlin, A. J. Logsdail, S. M. Woodley, C. R. A. Catlow, M. J. Powell, R. G. Palgrave, I. P. Parkin, G. W. Watson, T. W. Keal, P. Sherwood, A. Walsh and A. A. Sokol, *Nature Materials*, 2013, **12**, 798-801.

22.   X. Meng, D.-W. Shin, S. M. Yu, J. H. Jung, H. I. Kim, H. M. Lee, Y.-H. Han, V. Bhoraskar and J.-B. Yoo, *CrystEngComm*, 2011, **13**, 3021-3029.

23.   C. Yan and D. Xue, *Advanced Materials*, 2008, **20**, 1055-1058.

24.   M. Marzo, P. Carniti and A. Gervasini, *Chimica Oggi-Chemistry Today*, 2012, **30**, 22-24.

25.   Z. Wang, Y. Hu, W. Wang, X. Zhang, B. Wang, H. Tian, Y. Wang, J. Guan and H. Gu, *International Journal of Hydrogen Energy*, 2012, **37**, 4526-4532.

26.   A. Le Viet, M. V. Reddy, R. Jose, B. V. R. Chowdari and S. Ramakrishna, *Journal of Physical Chemistry C*, 2010, **114**, 664-671.

27.   L. Peng, L. Hu and X. Fang, *Advanced Materials*, 2013, **25**, 5321-5328.

28.   X. Fang, L. Hu, K. Huo, B. Gao, L. Zhao, M. Liao, P. K. Chu, Y. Bando and D. Golberg, *Advanced Functional Materials*, 2011, **21**, 3907-3915.

29.   H. Liu, Z. Zhang, L. Hu, N. Gao, L. Sang, M. Liao, R. Ma, F. Xu and X. Fang, *Advanced Optical Materials*, 2014, **2**, 771-778.

30.   H. Zhang, Y. Li, Y. Wang, P. Liu, H. Yang, X. Yao, T. An, B. J. Wood and H. Zhao, *Journal of Materials Chemistry A*, 2013, **1**, 6563-6571.

31.   I. Sieber, H. Hildebrand, A. Friedrich and P. Schmuki, *Electrochemistry Communications*, 2005, **7**, 97-100.

32.   W. Wei, K. Lee, S. Shaw and P. Schmuki, *Chemical Communications*, 2012, **48**, 4244-4246.

33.   K. Lee, Y. Yang, M. Yang and P. Schmuki, *Chemistry – A European Journal*, 2012, **18**, 9521-9524.

34. B. Tzvetkov, M. Bojinov, A. Girginov and N. Pébère, *Electrochimica Acta*, 2007, **52**, 7724-7731.
35. H. Störmer, A. Weber, V. Fischer, E. Ivers-Tiffée and D. Gerthsen, *Journal of the European Ceramic Society*, 2009, **29**, 1743-1753.
36. J. E. Yoo and J. Choi, *Electrochimica Acta*, 2010, **55**, 5142-5147.
37. A. Dragan, A. E. Graham and C. D. Geddes, *Journal of Fluorescence*, 2014, **24**, 397-402.
38. M. Wang, Y. Liu and H. Yang, *Electrochimica Acta*, 2012, **62**, 424-432.
39. G. Agarwal and G. B. Reddy, *Journal of Materials Science: Materials in Electronics*, 2005, **16**, 21-24.
40. L. I. U. Dawei, X. Peng, Z. Yunhuai, G. B. B, Z. Qifeng, G. U. O. Qing, C. Richard and C. A. O. Guozhong, *Journal of Physical Chemistry. C*, 2008, **112**, 11175-11180.
41. J. R. Gonzalez, R. Alcantara, F. Nacimiento, G. F. Ortiz and J. L. Tirado, *CrystEngComm*, 2014, **16**, 4602-4609.
42. L. Kronik and Y. Shapira, *Surface Science Reports*, 1999, **37**, 1-206.
43. X. Fang, Y. Bando, M. Liao, U. K. Gautam, C. Zhi, B. Dierre, B. Liu, T. Zhai, T. Sekiguchi, Y. Koide and D. Golberg, *Advanced Materials*, 2009, **21**, 2034-2039.
44. K. Deng, H. Lu, Z. Shi, Q. Liu and L. Li, *ACS Applied Materials & Interfaces*, 2013, **5**, 7845-7851.
45. S. E. Ahn, J. S. Lee, H. Kim, S. Kim, B. H. Kang, K. H. Kim and G. T. Kim, *Applied Physics Letters*, 2004, **84**, 5022-5024.
46. J. Zhou, Y. Gu, Y. Hu, W. Mai, P.-H. Yeh, G. Bao, A. K. Sood, D. L. Polla and Z. L. Wang, *Applied Physics Letters*, 2009, **94**, 191103.